

Supplemental Material

Two-dimensional ferroelectric metal for electrocatalysis

Changming Ke,^{1,2,3} Jiawei Huang,^{1,4} and Shi Liu^{1,2,3,*}

¹*School of Science, Westlake University,*

Hangzhou, Zhejiang 310024, China

²*Institute of Natural Sciences, Westlake Institute for Advanced Study,*

Hangzhou, Zhejiang 310024, China

³*Key Laboratory for Quantum Materials of Zhejiang*

Province, Hangzhou Zhejiang 310024, China

⁴*Zhejiang University, Hangzhou, Zhejiang 310058, China*

I. OUT-OF-PLANE POLARIZATION OF 2D FERROELECTRICS

Unlike the macroscopic polarization of a crystalline solid being well defined only for an insulator, the polarization of a bounded and charge-neutral sample is a trivial quantity for both insulator and metal, simply determined by the asymmetry of the charge distribution, i.e., electric dipole moment (μ). For the two-dimensional (2D) ferroelectric (FE) studied in this work as shown in FIG. S1, the out-of-plane polarization (\mathcal{P}_{OP}) is represented by the out-of-plane dipole moment defined as:

$$\mu_{\text{OP}} = \int (\mathbf{r}_z - R_z) \rho^{\text{ion+ele}}(\mathbf{r}) d\mathbf{r}_z \quad (1)$$

where R_z is the z -component of the geometry center of the 2D sheet and $\rho^{\text{ion+val}}$ is the total charge density of ions and electrons.

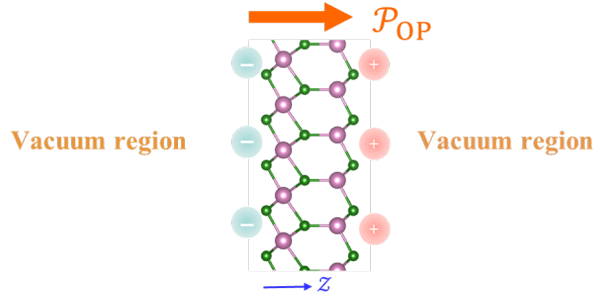


FIG. S1. Schematic of out-of-plane electric dipole moment in monolayer $\alpha\text{-In}_2\text{Se}_3$.

* liushi@westlake.edu.cn

II. ROBUSTNESS OF \mathcal{P}_{OP} AND FERROELECTRIC METALICITY AGAINST DEFECTS

The proposed design principle demonstrated with stacked 2D FEs goes beyond the rigid band model and is robust against various extrinsic effects such as defects. The core of the design principle illustrated in Fig. 1 is the depolarization field (\mathcal{E}_d) arising from the persistent out-of-plane polarization (\mathcal{P}_{OP}). Because the surfaces of 2D materials are intrinsically stable, free of dangling bonds, the depolarization field is also more robust against defects. We perform calculations to study the effects of defects on the magnitude of \mathcal{P}_{OP} and electronic structures of monolayer and bilayer $\alpha\text{-In}_2\text{Se}_3$. A few configurations with vacancies located at four different lattice sites shown in Fig.S2 are considered. Table S1 reports the values of out-of-plane dipole moment (μ_{OP}) for deficient monolayer and bilayer systems, demonstrating persistent polarization even at such high defect concentration ($8.02 \times 10^{13}/\text{cm}^2$). Fig. S2 also shows the band structures of bilayer $\alpha\text{-In}_2\text{Se}_3$ with vacancies at different sites, all exhibiting metallic behavior with nonzero density of states at Fermi level, thus supporting the robustness of ferroelectric metallicity against defects.

TABLE S1. Out-of-plane dipole moment of a 2×2 supercell (μ_{OP}) of deficient monolayer and bilayer $\alpha\text{-In}_2\text{Se}_3$ at a defect concentration of $8.02 \times 10^{13}/\text{cm}^2$ modeled with a 3×3 supercell.

	monolayer	bilayer
V_{Se1}	0.28	0.40
V_{In1}	0.28	0.48
V_{In2}	0.40	0.48
V_{Se2}	0.36	0.24

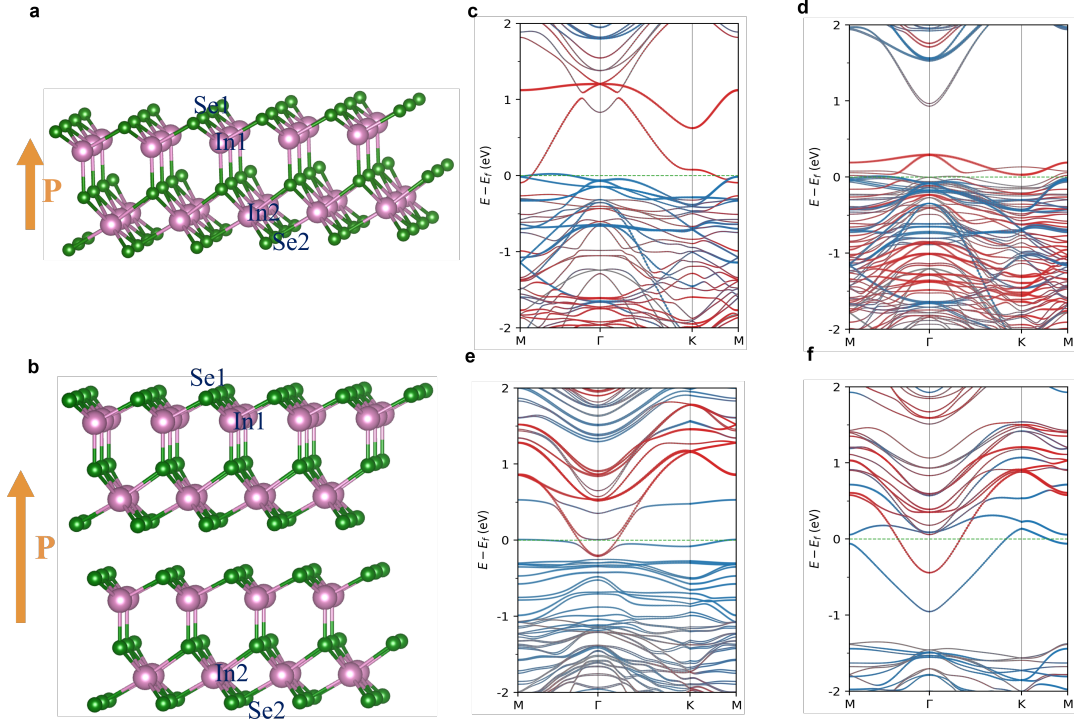


FIG. S2. Lattice sites of (a) monolayer (b) bilayer α - In_2Se_3 hosting vacancy. Projected band structures of deficient bilayer α - In_2Se_3 with (c) $V_{\text{Se}1}$, (d) $V_{\text{In}1}$, (e) $V_{\text{In}2}$, and (f) $V_{\text{Se}2}$. Atomic orbital contributions from \mathcal{P}^+ and \mathcal{P}^- surfaces are colored in red and blue, respectively.

III. ADSORPTION ENERGY CALCULATIONS

For adsorption energy calculations, three symmetry unique sites on $\alpha\text{-In}_2\text{X}_3$ surface are considered in this work, namely, top, bridge, and 3-fold sites, as shown in Fig. S3. And the adsorption energies of O on these sites of 1L, 2L and 3L $\alpha\text{-In}_2\text{Se}_3$ are listed in Table S2, with the adsorption energy defined as:

$$\Delta E_i = E_{i,\text{surf}} - E_{\text{surf}} - E_i \quad (2)$$

Here, $E_{i,\text{surf}}$ is the energy of a surface with an adsorbed specie i (e.g., O), and E_{surf} is energy of a clean surface, E_i is the energy of an isolated molecule i . Because the 3-fold site is most bonded, it has the lowest adsorption energy and thus considered as the activation site for electrocatalysis. To improve the reproducibility, We now offer key structural files via github. The link to the files is https://github.com/sliuththeorygroup/structure/tree/main/L21_polar_metal_catalysis

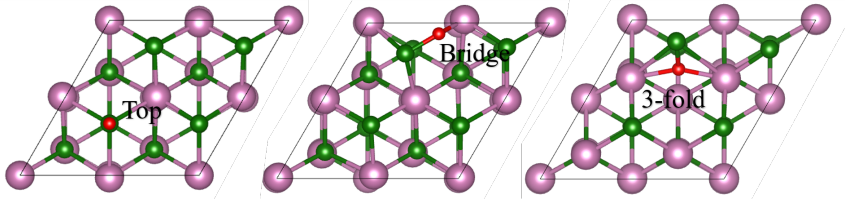


FIG. S3. Adsorption sites of O on the surface of $\alpha\text{-In}_2\text{Se}_3$

TABLE S2. Oxygen adsorption energies (eV) on 1L, 2L, and 3L $\alpha\text{-In}_2\text{Se}_3$.

Surface/Site	1L	2L	3L
\mathcal{P}^+ /Top	-2.73	-2.75	-2.71
\mathcal{P}^+ /3-fold	-3.41	-3.42	-3.41
\mathcal{P}^+ /Bridge	-3.39	-2.92	-3.38
\mathcal{P}^- /Top	-3.01	-3.10	-3.15
\mathcal{P}^- /3-fold	-3.69	-3.81	-3.89
\mathcal{P}^- /Bridge	-3.66	-3.74	-3.81

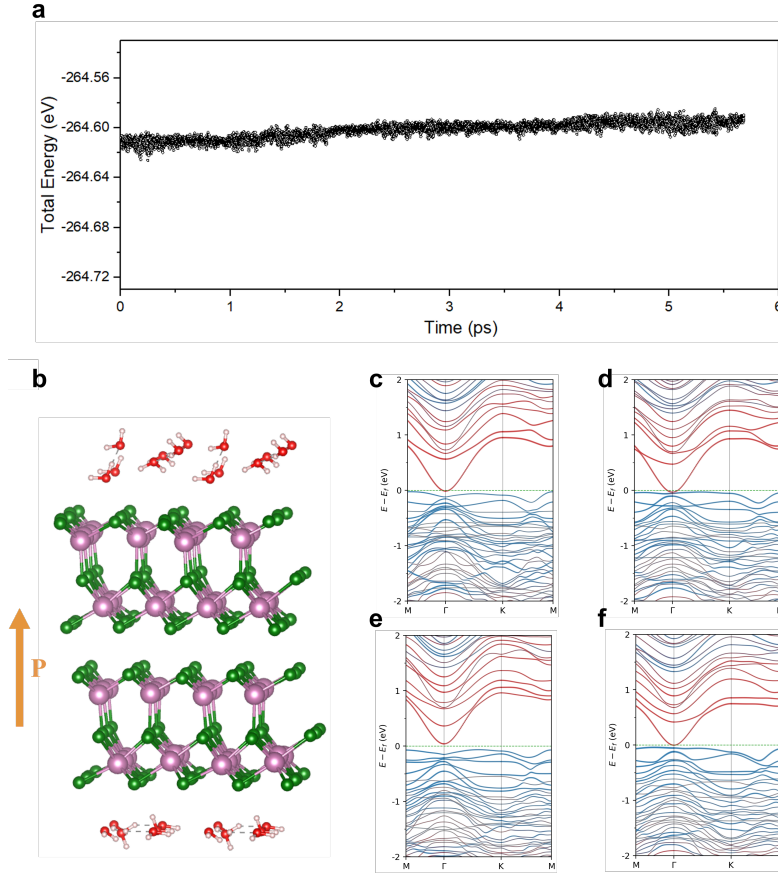


FIG. S4. (a) Energy evolution as a function of time for a 5 ps AIMD trajectory. (b) Typical configuration of bilayer α - In_2Se_3 in water. PBE band structures of snapshots from AIMD simulations at (b) 2 ps, (c) 3 ps, (d) 4 ps, and (e) 5 ps after equilibrium.

IV. STABILITY OF FERROELECTRIC METALLICITY IN WATER

It is important to check the validity of the proposed ferroelectric electrocatalysis in a more realistic setup. We investigate the stability of ferroelectric metallicity in the presence of a polarized medium such as water. The *ab initio* molecular dynamic simulation (AIMD) of bilayer α - In_2Se_3 sandwiched by monolayer H_2O (1 molecule/unit cell) is performed, and our calculations show that the interaction of H_2O with α - In_2Se_3 surfaces is weak, implying a physical adsorption. We obtained a AIMD trajectory of about 5 ps after equilibrium at 298 K, with a typical snapshot presented in Fig.S4(b). The band structures of a few snapshots are calculated by PBE (Fig.S4), revealing persistent semimetal nature (or tiny band gap) similar to bilayer α - In_2Se_3 in vacuum. This confirms the stability of ferroelectric metallicity

under water environment.

V. STABILITY OF FERROELECTRIC METALLICITY WITH O/H ADSORPTION

Different from the physical adsorption of H_2O , O and H covalently and strongly adsorb on $\alpha\text{-In}_2\text{Se}_3$ surfaces. In principle, the adsorption energy should be computed at a low surface coverage which requires the usage of a large supercell such that the fictitious interaction between the adsorbate and its mirror image is negligible. Our benchmark calculations using a 2×2 supercell revealed that both \mathcal{P}^+ and \mathcal{P}^- surfaces of multilayer $\alpha\text{-In}_2\text{Se}_3$ are stable in the presence of chemisorbed O with a high surface coverage of 25%. The \mathcal{P}^- surface with a quarter monolayer coverage of H is also stable. Interestingly, the same surface coverage of H on the \mathcal{P}^+ surface, however, will suppress the out-of-plane polarization and drive an $\alpha\text{-}\beta'$ phase transition. We further studied the effects of strain on the stability of multilayer $\alpha\text{-In}_2\text{Se}_3$ with O/H adsorption and found that a moderate uniaxial tensile strain of 2% is enough to enhance the stability for H adsorbed on \mathcal{P}^+ . To quantify the adsorption energy of O and H at a realistic surface coverage and the same strain condition while being computationally affordable, we investigated the adsorption of O and H on multilayer $\alpha\text{-In}_2\text{Se}_3$ uniaxially strained by 2% with a surface coverage of 12.5%. As shown in Fig.S5, the projected band structures of bilayer $\alpha\text{-In}_2\text{Se}_3$ with adsorbed O and H reveal nonzero density of states at the Fermi level, indicating the preserved ferroelectric metallicity.

TABLE S3. Effects of uniaxial tensile strain on the adsorption energy (eV) of H/O on the \mathcal{P}^- surface of multilayer $\alpha\text{-In}_2\text{Se}_3$.

	$\Delta E(\eta = 0)$	$\Delta E(\eta = +2\%)$	$\Delta E(\eta = +2\%) - \Delta E(\eta = 0\%)$
1L	-1.60	-1.64	-0.042
H adsorption 2L	-2.10	-2.19	-0.096
3L	-2.52	-2.61	-0.086
1L	-3.69	-3.76	-0.062
O adsorption 2L	-3.81	-3.87	-0.064
3L	-3.89	-3.92	-0.03

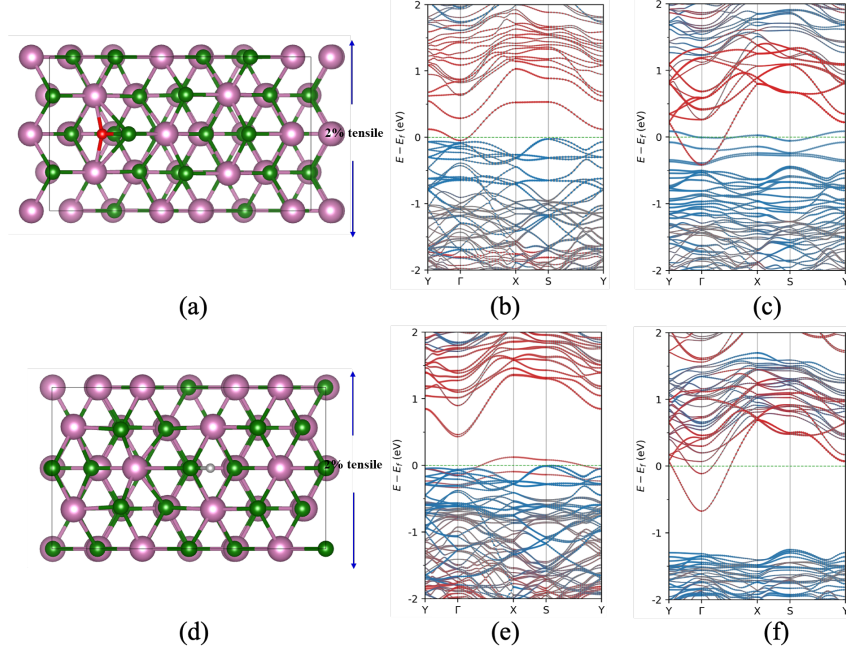


FIG. S5. Optimized geometry and band structure of O and H adsorbed on bilayer α - In_2Se_3 uniaxially strained by 2%. (a) Top view of O adsorbed on the \mathcal{P}^+ surface. Projected band structures of O adsorbed on (b) \mathcal{P}^+ surface and (c) \mathcal{P}^- surface. (d) Top view of H adsorbed on the \mathcal{P}^+ surface. Projected band structures of H adsorbed on (e) \mathcal{P}^+ surface and (f) \mathcal{P}^- surface.

VI. ELECTRICAL TRANSPORT PROPERTIES OF LAYERED α -In₂Se₃

The issues of poor charge transport and low conductivity of wide-band-gap ferroelectrics make them unsuitable for the electrocatalytic reaction to occur. Here, we find that layered α -In₂Se₃ have improved electrical conductivity, as shown in Fig.S7, thus potentially enabling electrocatalysis with tunable carrier type.

To give a quantitative perspective of electrical transport properties, the intrinsic carrier density, conductivity, and mobility of α -In₂Se₃ systems, Pt slab, bulk Pt, Al, Cu, and Si, all computed from the semiclassical Boltzmann transport theory, are listed in Table S4. Typical electron mobility at room temperature (300 K) in metals like gold, copper, and silver is 10-50 cm²/V/s, comparable with the value of bulk Pt (30 cm²/V/s) estimated here. The computed value of the electron mobility of Si is 1288 cm²/V/s, consistent with the measured value at the order of 1000 cm²/V/s (https://en.wikipedia.org/wiki/Electron_mobility). The decent agreements between theory and experiments for metals and semiconductors indicate the validity of computed carrier mobility. The high conductivity of noble metal, Pt, is owe to its high carrier density, however, its carrier mobility is very low. Interestingly, the Pt slab (≈ 4.9 Å) has reduced mobility compare to the bulk. The low conductivity of silicon is caused by its low carrier density, despite the high mobility. Notably, the ferroelectric metal represented by bilayer and trilayer α -In₂Se₃ possess both high carrier density and mobility, beneficial for electrocatalysis.

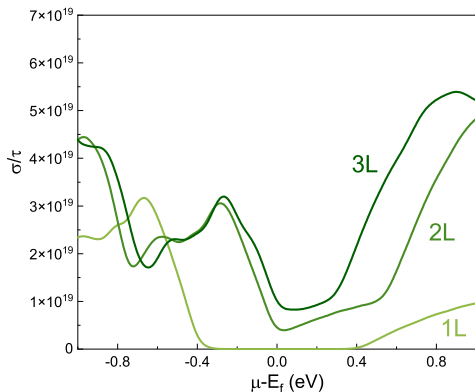


FIG. S6. Electrical conductivity (σ) with respect to scattering time (τ) within the plane versus the chemical potential for 1L, 2L, and 3L α -In₂Se₃.

TABLE S4. Intrinsic carrier density (n) in $1/\text{cm}^3$, conductivity (σ) in S/m, and mobility (μ) in $\text{cm}^2/\text{V}/\text{sec}$ at 300 K calculated using the semiclassical Boltzmann transport theory, assuming a carrier relaxation time of 20 fs for $\alpha\text{-In}_2\text{Se}_3$ and Pt, and 200 fs for Si [*PRB*, 97, 045201 (2018)].

Experimentally measured electron mobility is 1400 in Si and 10-50 in metals like Ag and Cu.

	n	σ	μ
Monolayer	1.57×10^{16}	10.2	61
Bilayer	1.33×10^{19}	9.2×10^4	432
Trilayer	1.75×10^{19}	1.9×10^5	695
Pt (slab)	6.40×10^{22}	6.9×10^6	7
Pt (bluk)	6.40×10^{22}	2.6×10^7	25
Al	6.05×10^{22}	6.2×10^7	64
Cu	8.4×10^{22}	3.3×10^7	25
Si	1×10^{10}	2.06×10^{-4}	1288

VII. ELECTROSTATIC MODEL OF POLAR SLAB

We explain in detail that a simple electrostatic model can not explain the key physics of interest of current system, adsorption energy of small molecules on polar surfaces of stacked 2D FEs. Previous studies [*PRL* 107, 187602 (2011), *Rep. Prog. Phys.*, 81, 036502 (2018)] suggested that the concentration (θ) of O^* (denoting O atom adsorbed on a charged surface ion) obeys the following relationship

$$\theta(\phi) = \frac{\alpha(\phi)}{1 + \alpha(\phi)}, \alpha(\phi) = (P_{O_2})^{1/2} \exp\left(\frac{-\Delta G_{O^*}^0 - eZ_{O^*}\phi}{k_b T}\right)$$

Here, P_{O_2} is the partial pressure of oxygen gas, Z_{O^*} is the charge of surface ion adsorbed by O, $\Delta G_{O^*}^0$ is the standard free energy of O^* formation at $P_{O_2} = 1$ bar and zero potential (ϕ). According to this electrostatic model, negatively charged O^* prefers to adsorb on the \mathcal{P}^+ surface. Similarly, positively charged H^* prefers to adsorb on the \mathcal{P}^- surface. However, our DFT calculations (Fig. 4a in the manuscript) clearly showed that both H and O have stronger interactions with the \mathcal{P}^- surface. We further demonstrated that the adsorption energy is dictated by the energy difference between the p -band center of surface atoms and the frontier orbital of adsorbates (Fig. 4b in the manuscript). Therefore, unlike the polar surfaces of ferroelectric slabs whose properties are mainly controlled by the charge compensation processes for depolarization screening, the physical and chemical properties of polar surfaces of stacked 2D FEs are determined by the intrinsic electronic structure that couples directly with the strength of unscreened depolarization field.

VIII. FREE ENERGY CALCULATION OF OXYGEN REDUCTION REACTION

According to the scaling relationship of OH_x [*PRL*, 99, 016105 (2007)], the adsorption energy of OH (ΔE_{OH}) can be estimated from the adsorption energy of O as:

$$\Delta E_{\text{OH}} = 0.50 \times \Delta E_{\text{O}} - 0.23(\text{eV})$$

The adsorption energies of OH on layered $\alpha\text{-In}_2\text{Se}_3$ estimated from ΔE_{O} are listed in Table S5. The reaction heat ($\Delta\mathcal{H}$) of a dissociative reaction on surface is calculated following the protocol developed in *JACS*, 125, 3704 (2003):



where * denotes a site on the surface and E_i^{gs} is the energy of an isolated molecule i . For the simple dissociative mechanism of oxygen reduction at a fuel cell cathode, the reaction free energy (ΔG) under an electrode potential U is obtained using:

$$\Delta G_0(U) = \Delta\mathcal{H}_{\text{O}} - 2eU + 0.01 \text{ eV}$$

$$\Delta G_1(U) = \Delta\mathcal{H}_{\text{OH}} - \Delta\mathcal{H}_{\text{O}} + eU - 0.26 \text{ eV}$$

$$\Delta G_2(U) = -\Delta\mathcal{H}_{\text{OH}} + eU + 0.25 \text{ eV}$$

where ΔG_m ($m = 0, 1, 2$) is the reaction free energy for the three elementary steps as shown in Figure 4c of the manuscript.

TABLE S5. Adsorption energy (ΔE in eV) of O and OH on layered In_2Se_3 , In_2Te_3 , and Pt estimated using the scaling relationship.

	ΔE_{O}	ΔE_{OH}		ΔE_{O}	ΔE_{OH}
$\text{In}_2\text{Se}_3/1\text{L}/\mathcal{P}^+$	-3.49	-1.97	$\text{In}_2\text{Te}_3/1\text{L}/\mathcal{P}^+$	-3.98	-2.22
$\text{In}_2\text{Se}_3/1\text{L}/\mathcal{P}^-$	-3.76	-2.11	$\text{In}_2\text{Te}_3/1\text{L}/\mathcal{P}^-$	-4.23	-2.35
$\text{In}_2\text{Se}_3/2\text{L}/\mathcal{P}^-$	-3.87	-2.17	$\text{In}_2\text{Te}_3/2\text{L}/\mathcal{P}^-$	-4.28	-2.37
$\text{In}_2\text{Se}_3/3\text{L}/\mathcal{P}^-$	-3.91	-2.19	$\text{In}_2\text{Te}_3/3\text{L}/\mathcal{P}^-$	-4.34	-2.40
Pt	-4.56	-2.51			

IX. BAND BENDING IN 2D FERROELECTRICS

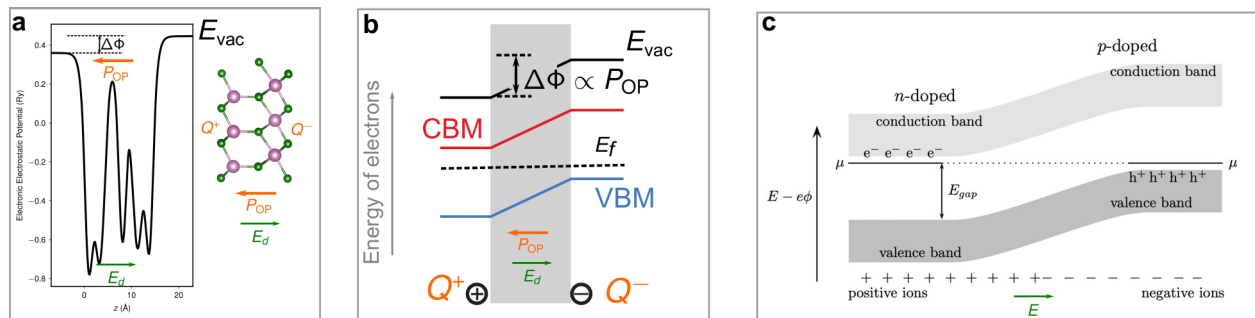


FIG. S7. (a) Electronic electrostatic potential for monolayer α - In_2Se_3 computed with DFT. Band bending in (b) a 2D ferroelectric monolayer and (c) an unbiased p - n junction (taken from page 201 of “The Oxford Solid State Physics” by Steven H. Simon).